UCSF
UC San Francisco Electronic Theses and Dissertations

Title
Evaluating the Performance of Augmented Reality in Displaying 3D Holographic Models Derived from MR Techniques

Permalink
https://escholarship.org/uc/item/6sm5r3vs

Author
Chang, Frank

Publication Date
2018

Peer reviewed|Thesis/dissertation

eScholarship.org Powered by the California Digital Library
University of California

Evaluating the Performance of Augmented Reality in Displaying 3D Holographic Models Derived from MR Techniques

by

Frank Chang

THESIS

Submitted in partial satisfaction of the requirements for the degree of

MASTER OF SCIENCE

in

Biomedical Imaging

in the

GRADUATE DIVISION

of the

[redacted]

Copyright 2018

by

Frank Chang

Acknowledgements

Thank you, Jesse, for leading me to the field of AR. And thank you to my thesis committee for the guidance and inspiration. To Yu-Lin and Pao, all of this would not have been possible without the useful insight both of you provided me. Finally, I give my thanks to the UCSF MSBI program for all the support.

Evaluating the Performance of Augmented Reality in Displaying 3D Holographic Models Derived from MR Techniques

Frank Chang

Objective: The primary objective of this study is to investigate the performance of augmented reality (AR) in representing and displaying 3D holographic models derived from 3D MR acquisitions. In addition, the existing picture archiving and communication system (PACS) will be examined as well.

Methods: A compatible phantom model for the 3.0T standard bore GE MRI scanner was used and fiducial markers set at various known distances were placed on the surface of the model. The distances were measured using a digital caliper, establishing the reference gold standard. Five separate configurations were created using the same phantom model by rearranging the fiducial markers. A set of six total measurements between fiducial markers were made in each configuration: two along the x-direction, two along the y-direction, and two along the z-direction. Four different 3D MR sequences were implemented to scan each configuration. The resulting 3D MR images of each sequence for every configuration were stored as digital imaging and communications in medicine (DICOM) files and sent to PACS. The corresponding six distances were then measured using the built-in PACS ruler tool. Open-source 3D rendering software programs were used to translate the DICOM files into 3D models, which were then loaded onto an AR platform. The 3D models were displayed as holograms and the overlaid distances between the fiducial markers were measured using a physical digital caliper. Since the assumptions for parametric statistical analysis were violated, the nonparametric statistical method was adopted to examine the statistical differences among the three groups (gold standard, PACS, and AR).

Results: The results showed no statistically significant difference between AR measurements and gold standard measurements ($p = 0.6208$). However, a statistically significant difference between PACS measurements and gold standard measurements ($p = 0.0118$) was present.

Conclusion: Distance measurements in AR models derived from MRI scans show no statistically significant difference compared to gold standard measurements. AR can be used to accurately measure distance for surgical planning and clinical use.

Table of Contents

List of Tables

List of Figures

Chapter 1

Introduction

Augmented reality (AR) is a powerful application that allows physicians to visualize and interact with patient data. By definition, augmented reality is a real-time interactive experience of the real-world environment using computer-generated perceptual information. The information can be overlaid by adding to or masking from the real-world environment. It is important to note that AR is different from virtual reality (VR). VR is also a real-time interactive experience using computer-generated perceptual information, but it takes place completely in a simulated environment. Therefore, AR is the preferred modality to visualize organ anatomy as patients are real objects and are part of the real-world environment. Multiple studies have tested the feasibility of AR in the clinical setting with promising results, but the performance of this modality has yet to be explored in more detail [1]. To date, augmented reality has been carried out using techniques such as image projection and registration with an optical tracker [2,3]. These methods introduce unwanted projection and registration errors which could lead to misinterpretation of the true morphology of the anatomy or structure of interest. Further robust methods for developing better representations of computer-generated information could benefit current treatment and diagnostic workflows, ultimately improving the efficiency and standard of care. Recently, the use of holograms generated from 3D renderings has been introduced and this project will utilize the concept of holographic models for AR visualization.

Figure 1. Microsoft HoloLens (image via The Verge)

The Microsoft HoloLens hardware is a headset device that is completely wire-free and Wi-Fi enabled (Figure 1). It responds to a series of hand gestures as well as voice commands and can be paired with holographic augmentation software to display 3D holograms. These convenient features collectively allow for a smoother integration of the technology into the physician workflow. The ability of the HoloLens to make reproducible measurements as an instrument has already been characterized in the field of surgery [4]. In addition, the HoloLens is capable of accurately following hand gestures and voice commands for manipulation and interaction of 3D objects [5,6]. Together, the HoloLens has been demonstrated as a competent tool to assist surgeons and other medical professionals with preoperative surgical planning, such as the localization of subsurface vascular perforators, as well as intraoperative landmarking [6]. From a usability standpoint, the HoloLens, like many other AR devices, has received positive reception with users reporting ease of use and the intuitive nature of the technology [4,7].

Using AR to display 3D holographic models derived from computed tomography (CT) techniques was previously shown to be a reliable method with no statistically significant difference between reference measurements and AR measurements [8]. Because magnetic resonance (MR) imaging techniques offer superior soft tissue contrast, assessing how AR handles 3D holographic models derived from MR techniques could elucidate and unlock even more information about this specific technology for future clinical use. Thus, this particular project seeks to explore the performance of AR in representing and displaying 3D holographic models derived from 3D MR acquisitions. Since the picture archiving and communication system (PACS) is part of the current diagnostic workflow in radiology and imaging, this step will be included in the experimental pipeline as well.

Chapter 2

Methods

2.1 Pipeline

The overall experimental pipeline is shown in Figure 2. As will be discussed in detail later, measurements will be collected in three major phases: 1) using the physical phantom model to establish the reference gold standard (GS), 2) using the PACS system after the MR acquisitions, and 3) using the HoloLens to display the translated 3D holograms in AR derived from digital imaging and communications in medicine (DICOM) files. Thus, there will be a total of three forms of measurements: GS, PACS, and AR.

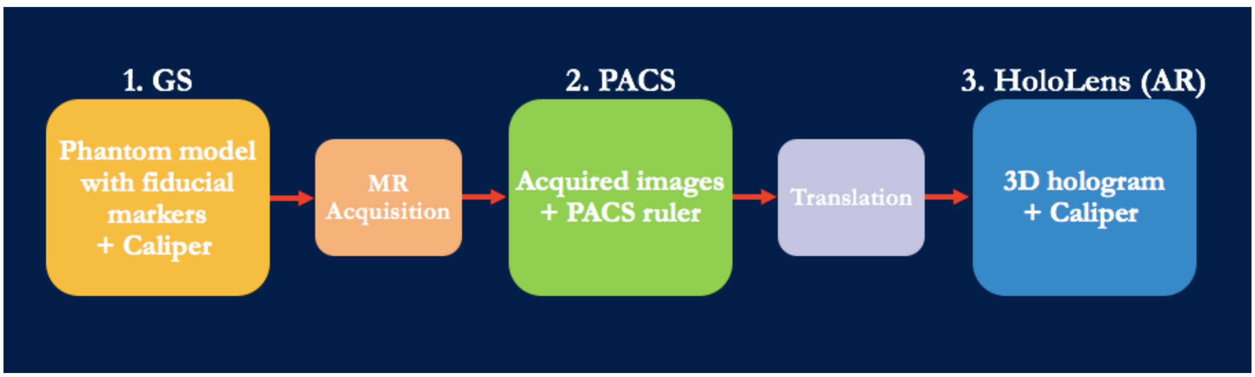

Figure 2. Experimental pipeline

2.2 Phantom Model

A compatible phantom model (Cubical Unified Phantom 5342681, GE Healthcare) for the GE MRI scanner was used throughout the data collection process (Figure 3). Five different phantom configurations (Configuration A-E) were made in total. For the first configuration, fiducial markers (MR-SPOT #121 and 122, Beekley Medical) were placed on the surface of the phantom model to form a total of two distances along each of the three directions of the cube: two in the x-direction, two in the y-direction, and two in the z-direction (Figures 4 & 5). An optional grid paper (Fast Find Grid, Webb Medical) was wrapped around the phantom model to guide and ensure accurate fiducial marker placement along each axis. A digital caliper (Model 01407A, Neiko Tools) was used to measure the six designated distances between the fiducial markers along each of the three directions (Figure 6). The rest of the four configurations were designed in the same way but with varying distances between the fiducial markers.

Figure 3. Compatible phantom model for the 3.0T GE MRI scanner

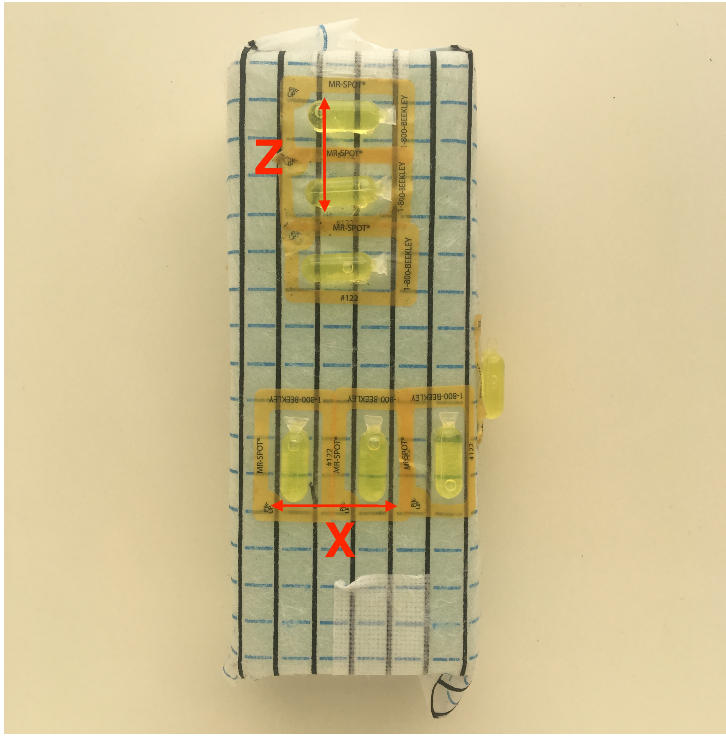

Figure 4. Fiducial markers placed along the x and z directions

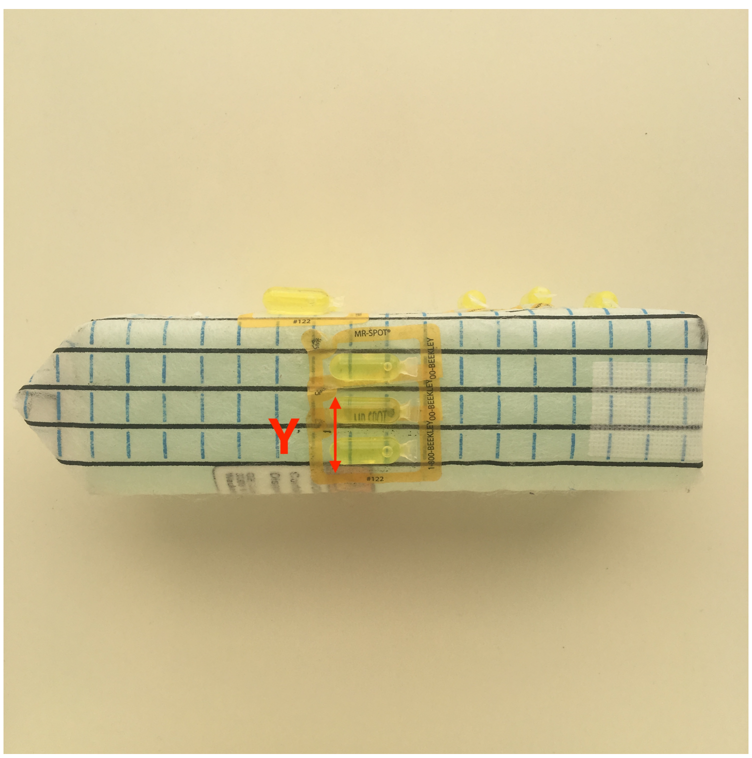

Figure 5. Fiducial markers placed along the y direction

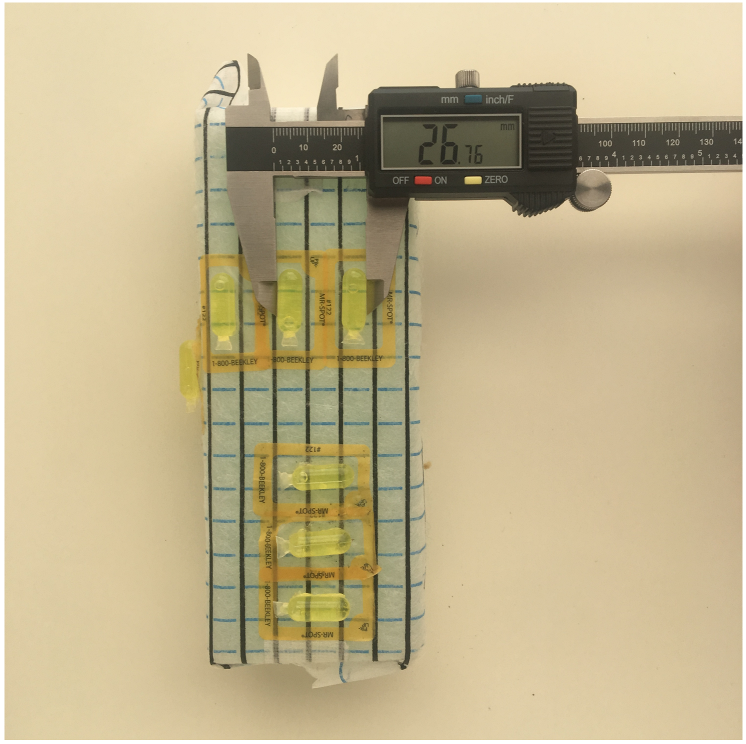

Figure 6. GS distance measurement using a digital caliper

The GS reference measurements for each of the five configurations are tabulated below in Table 1.

Direction \ Configuration	A	B	C	D	E
Z1	18.43 mm	25.84 mm	35.45 mm	45.25 mm	65.85 mm
Z2	31.53 mm	25.94 mm	37.09 mm	35.69 mm	45.69 mm
X1	30.91 mm	25.16 mm	37.27 mm	26.01 mm	55.63 mm
X2	17.75 mm	26.58 mm	16.48 mm	26.93 mm	46.72 mm
Y1	18.01 mm	16.85 mm	17.29 mm	16.96 mm	30.48 mm
Y2	31.25 mm	16.66 mm	24.99 mm	18.69 mm	28.74 mm

Table 1. GS distance measurements listed by configuration

2.3 MR Acquisition and PACS

The 3.0T normal bore GE MRI scanner and an 8-channel high resolution head coil were used for all MR acquisitions. Four 3D MR sequences were implemented to scan each of the five phantom configurations. The four sequences are 3D BRAVO, 3D CUBE T2, 3D FSPGR, and 3D LAVA-Flex. Default parameters using a 256 x 256 matrix with the thinnest slices possible were configured for all sequences except for LAVA-Flex (Figure 7). All LAVA-Flex sequences were run using a 200 x 200 matrix with the thinnest slices possible (Figure 8). Individual cross-sectional views were reformatted via multiplanar reconstruction (MRP) after each acquisition, and the resulting images were saved as DICOM files and sent to PACS. The PACS ruler tool was used to measure the distances between fiducial markers along the x and z directions in the coronal view, and the distances in the y direction were measured in the sagittal view (Figures 9 & 10). Windowing and leveling of the images were adjusted as needed to determine the slice with the greatest contrast between the markers and background. This process was repeated for the rest of the four configurations as well.

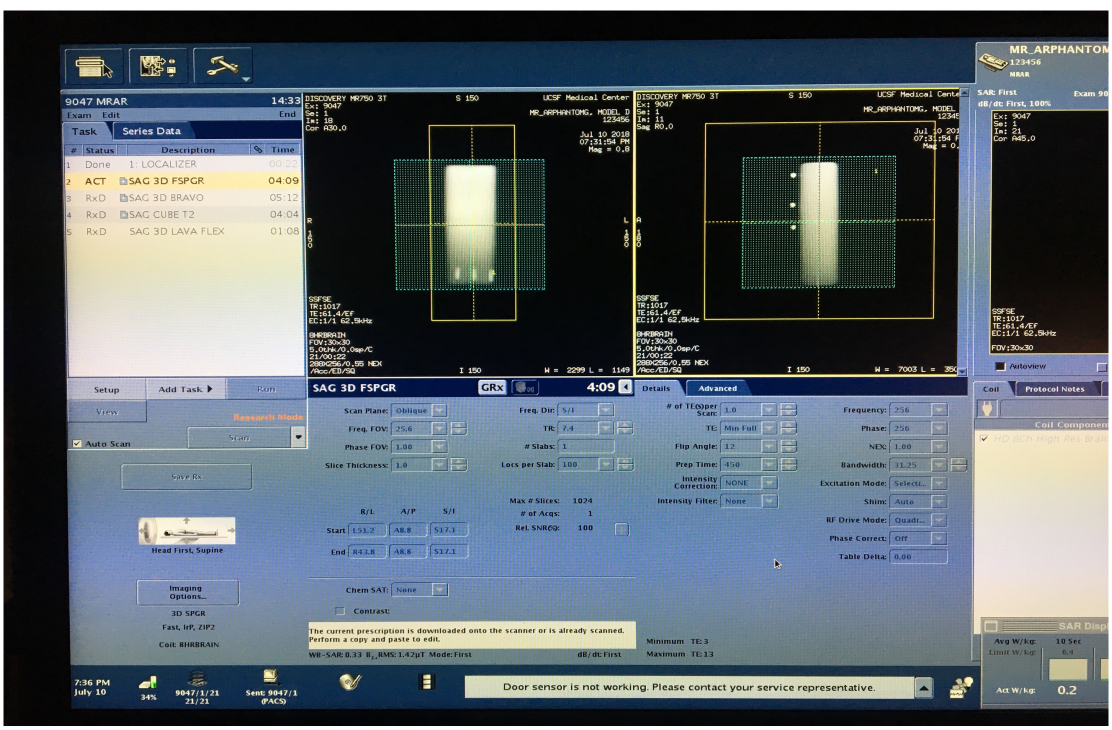

Figure 7. 3D FSPGR sequence acquisition parameters

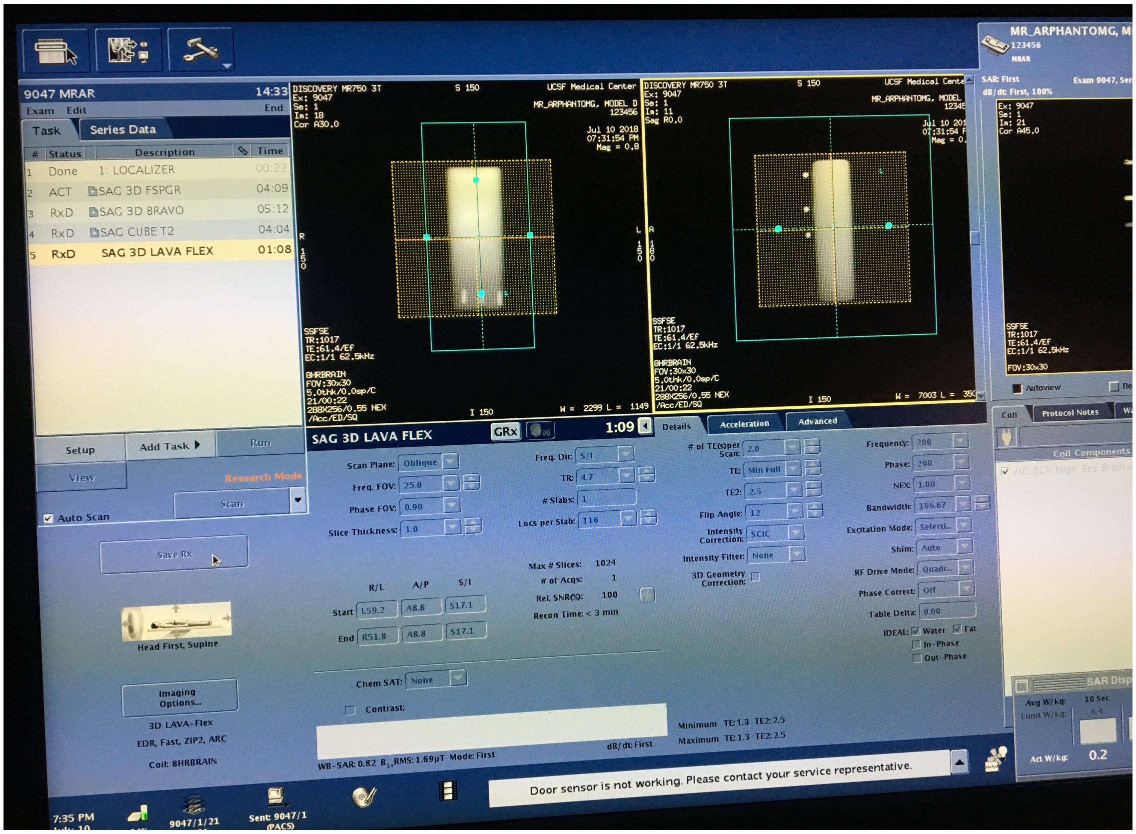

Figure 8. 3D LAVA-Flex sequence acquisition parameters

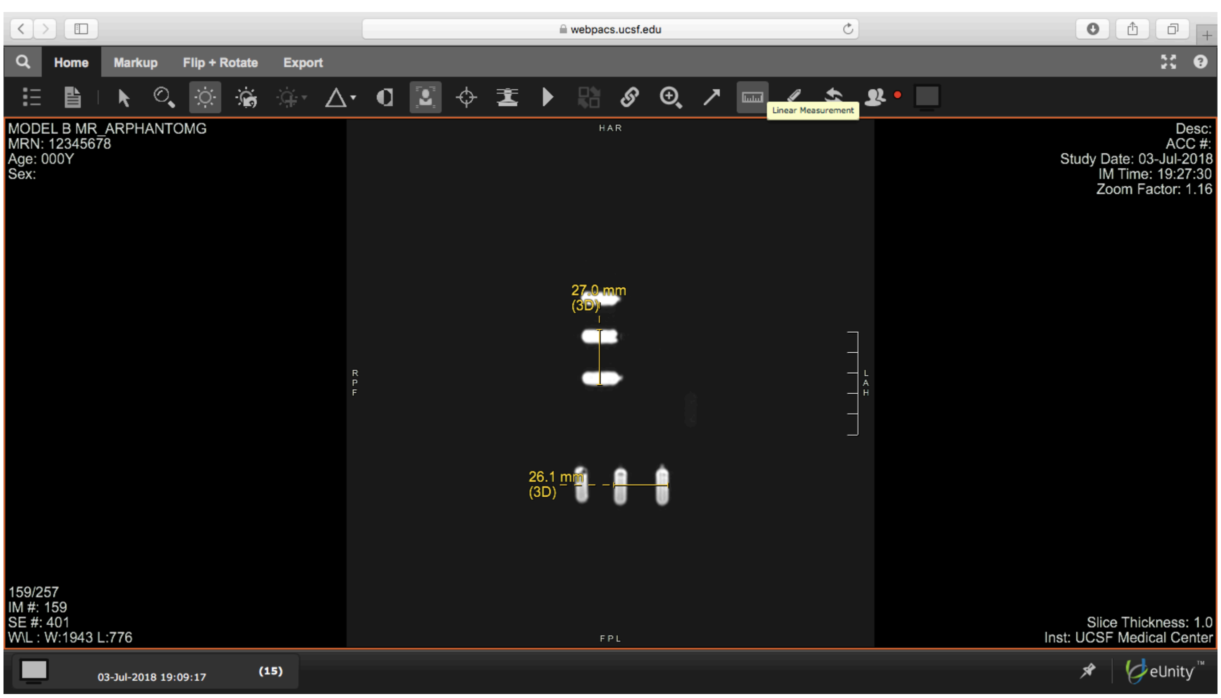

Figure 9. PACS interface for x and z direction measurements in coronal view

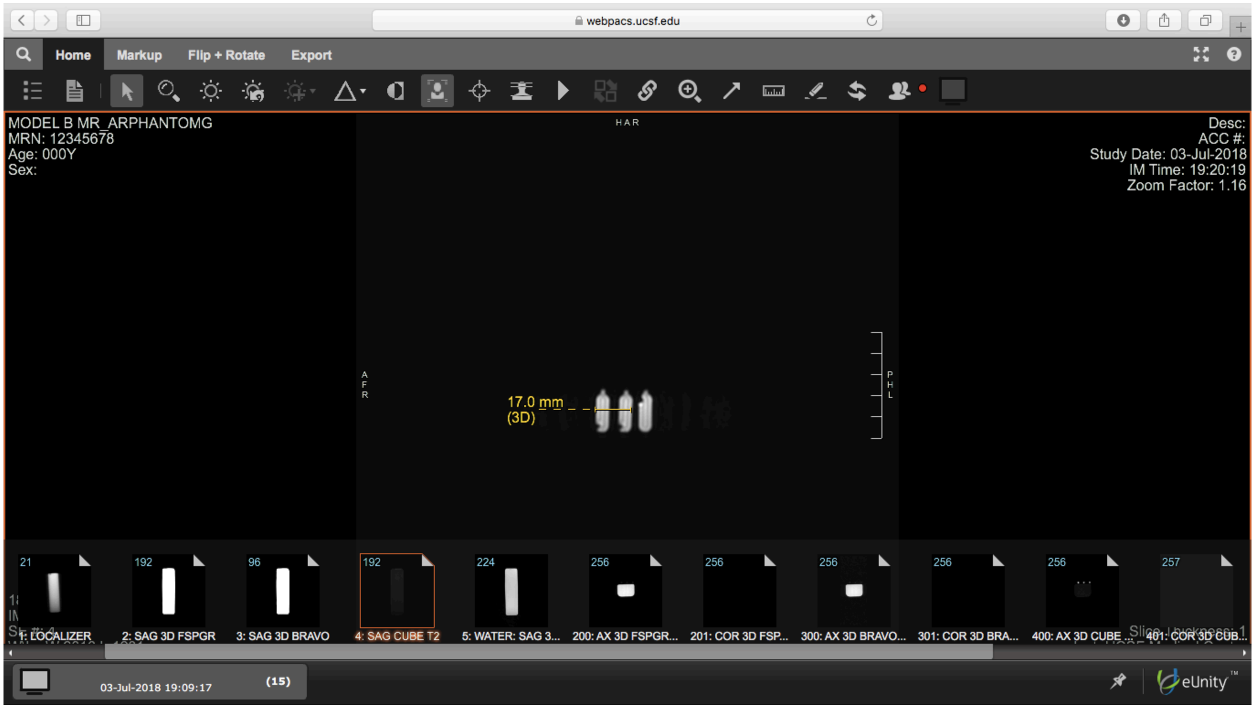

Figure 10. PACS interface for y direction measurements in sagittal view

2.4 Translation and AR

DICOM files for each 3D MR sequence acquisition were translated to 3D object files using open-source 3D rendering software MeshLab (http://www.meshlab.net) and Blender (https://www.blender.org). A decimation algorithm was applied as needed within the software interface for smoothing purposes and file reduction. Completed 3D renderings were exported as object files and loaded onto the HoloLens headset. From there, each object file was opened as 3D holograms using a series of hand gestures and voice commands. The “adjust” voice command generates adjustment bars and rings around the model, which can be dragged or pinched in all directions to manipulate the hologram (Figure 11). The hologram was then placed onto the table just like a normal physical phantom model would, and the same digital caliper that was used to measure GS references was used to measure the distances between the holographic fiducial markers along each of the three directions (Figure 12). The transparency of the hologram can be adjusted using the side buttons on the HoloLens to properly align the caliper to the desired set of fiducial markers.

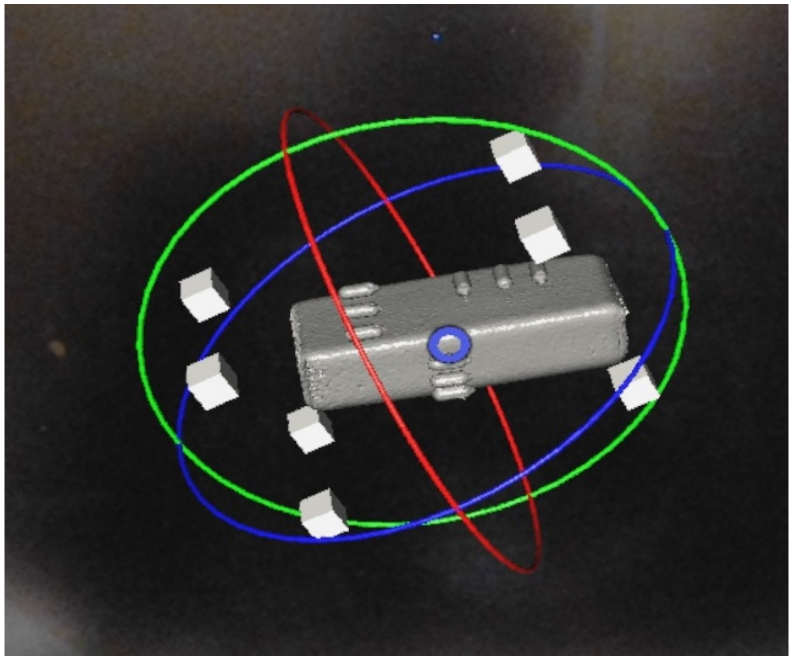

Figure 11. 3D hologram with adjustment bars and rings

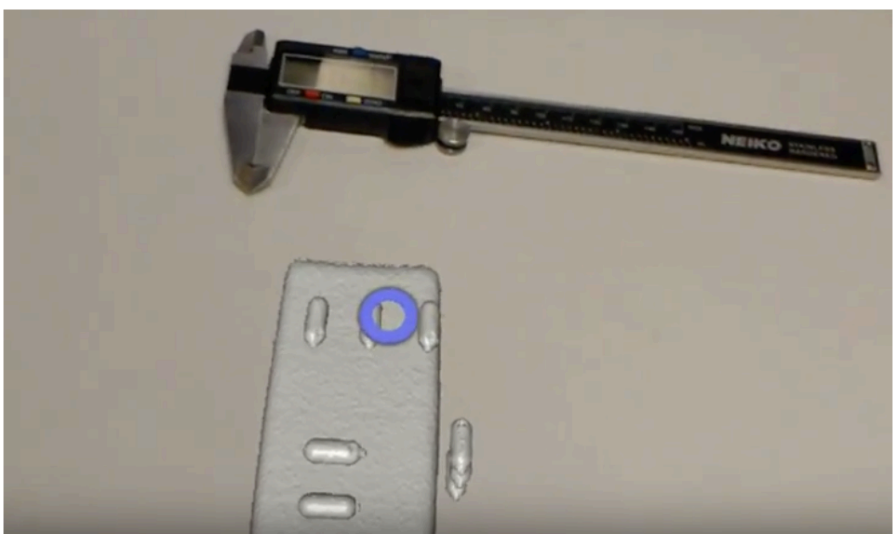

Figure 12. 3D hologram placed on the table for measuring with digital caliper

2.5 Referencing Distance Measurements

In order to evaluate how accurate AR and PACS measurements compare with GS reference measurements, the distance measurements along each of the three directions for the methods of measurements need to be referenced to the correct directional observation. For example, the distance measurement along direction X1 for AR needs to be matched to the distance measurement along X1 for GS. Similarly, the same applies for matching the distance measurement X1 for PACS to the distance measurement X1 for GS. To do this, a difference score was computed for each directional observation by subtracting the corresponding GS measurement from the AR measurement, and subtracting the corresponding GS measurement from the PACS measurement. The resulting difference scores will be dimensionless but will ensure that the correct distance comparisons with respect to the original referenced direction are made.

Chapter 3

Results

3.1 Methods of Measurements

The descriptive statistics of the difference scores for the methods of measurements variable are shown in Table 2.

	PACS	AR
Mean	-0.0809	0.0649
Standard Deviation	0.7865	0.8936
N	116	106

Table 2. Descriptive statistics of difference scores for methods of measurements

The Shapiro-Wilk tests were used to examine the normality of the data. The test results showed that the normal assumption for parametric testing does not hold ($p \leq 0.0138$). Therefore, nonparametric testing was adopted for examining the methods of measurements, and all of the testing was performed at a two-sided alpha level of 0.05. One-sample median test showed that there exists no significant difference between AR and GS ($p = 0.6208$). However, there exists a significant difference between PACS and GS ($p = 0.0118$). For the comparison between PACS and AR, the result of a two-sample median test indicated that there is a significant difference as well ($p = 0.0030$).

3.2 Sequences

The descriptive statistics of the difference scores for the sequences variable are listed in Table 3.

	3D BRAVO	3D CUBE T2	3D FSPGR	3D LAVA-Flex
Mean	0.1212	-0.0663	0.2128	-0.4291
Standard Deviation	0.8523	0.5433	1.0113	0.7645
N	59	60	60	43

Table 3. Descriptive statistics of difference scores for sequence types

The normality assumption does not hold for groups 3D CUBE T2 and 3D LAVA-Flex by the Shapiro-Wilk test ($p < 0.05$). Also, the homogeneity of variance assumption does not hold by the Levene's test ($p = 0.0077$). Therefore, nonparametric testing was adopted for the sequences variable. The Kruskal-Wallis test was performed on the sequences variable with a chi-square of 13.3508 and the result shows there exists some significant differences among the four levels of sequences ($p = 0.0039$). All pairwise comparisons among those four groups were further investigated by using two-sample Wilcoxon tests. For the six pairwise comparisons, only the 3D BRAVO vs. 3D LAVA-Flex sequence, 3D CUBE T2 vs. 3D LAVA-Flex sequence, and the 3D FSPGR vs. 3D LAVA-Flex sequence showed statistically significant differences ($p = 0.0041$, $p = 0.0110$ and $p = 0.0012$, respectively).

Additionally, the methods of measurements were investigated in each sequence type. Testing results revealed that there are some significant differences for the 3D CUBE T2 sequence as well as for the 3D LAVA-Flex sequence. For the 3D CUBE T2 sequence, one-sample median test showed there is a significant difference between PACS vs. GS measurements ($p = 0.0161$), and two-sample Wilcoxon test showed there is a significant difference between AR vs. PACS measurements ($p = 0.0017$). For the 3D LAVA-Flex sequence, one-sample median test presented a significant difference between AR and GS measurements ($p = 0.0490$).

Chapter 4

Discussion and Conclusion

Overall, results indicate that the HoloLens does a good job in representing 3D holographic models derived from 3D MR acquisition scans. AR can thus be used to accurately measure distances for applications such as surgical planning and clinical use. Differences reflected in PACS measurements agree with previous observations done for 3D holographic models derived from CT acquisition scans. This could be due to the fact that images in PACS are presented in 2D slices at fixed intensity levels which might pose a limitation to precisely determine fiducial marker locations. Sequence wise, it is expected that the 3D BRAVO and 3D FSPGR sequences have similar results as BRAVO is an FSPGR sequence used for scanning the brain. The 3D LAVA-Flex sequence uses a T1-weighted 3D GRE acquisition with a 2-point Dixon fat/water separation. Differences are expected for this sequence in the pairwise comparisons as the phantom and fiducial markers contain two different homogeneous substances both without traces of fat, giving little to no useful information in the resulting images. The significant differences presented for the 3D CUBE T2 sequence coincide closely with the results found in the comparisons among the methods of measurements, which means 3D CUBE T2 is the most consistent sequence with respect to the other three sequences explored. The significant difference seen between AR and GS measurements for the 3D LAVA-Flex sequence could be attributed to the lack of signal from some fiducial markers during the acquisitions, and hence a complete loss of the corresponding markers during the translation process into 3D holograms. A few other limitations in this study include the size and composition of the phantom used, file size limit for each object file loaded onto the HoloLens (20 MB), and lack of haptic feedback when interacting with the holograms. Future work could be explored by incorporating internal structures within the phantom, varying phantom sizes, as well as introducing different compositions. In addition, adjusting MR scanning setups and parameters—including bore size, magnet strength, types of sequences, and acquisition parameters—could offer more insight regarding the performance of AR in displaying holographic information derived from each respective acquisition.

References

1. Vávra, P., Roman, J., Zonča, P., et al. Recent Development of Augmented Reality in Surgery: A Review. *Journal of Healthcare Engineering*, *2017*, 4574172. http://doi.org/10.1155/2017/4574172 (2017).
2. Besharati Tabrizi, Leila & Mahvash, Mehran. Augmented reality–guided neurosurgery: accuracy and intraoperative application of an image projection technique. *Journal of Neurosurgery*. 123. 1-6. 10.3171/2014.9.JNS141001 (2015).
3. Yoshino, M., Saito, T., Kin, T., et al. A Microscopic Optically Tracking Navigation System That Uses High-resolution 3D Computer Graphics. *Neurologia Medico-Chirurgica*, *55*(8), 674–679. http://doi.org/10.2176/nmc.tn.2014-0278 (2015).
4. Adabi, K., Rudy, H., Stern, C. S., et al. Abstract: Optimizing Measurements in Plastic Surgery through Holograms with Microsoft Hololens. *Plastic and Reconstructive Surgery Global Open*, *5*(9 Suppl), 182–183. http://doi.org/10.1097/01.GOX.0000526428.21421.4a (2017).
5. Auvinet, E., Galna, B., Aframian, A., et al. O100: Validation of the precision of the Microsoft HoloLens augmented reality headset head and hand motion measurement. *Gait & Posture*. 57. 10.1016/j.gaitpost.2017.06.353 (2017).
6. Pratt, P., Ives, M., et al. Through the HoloLens™ looking glass: augmented reality for extremity reconstruction surgery using 3D vascular models with perforating vessels. *European Radiology Experimental*, *2*(1), 2. http://doi.org/10.1186/s41747-017-0033-2 (2018).
7. Liu, F., & Seipel, S. On the precision of third person perspective augmented reality for target designation tasks. *Multimedia Tools and Applications, 76*, 15279-15296 (2016).
8. Uribe, J., Vu, L., Howard, B., et al. Assessing accuracy and precision of 3D augmented reality holographic models derived from DICOM data [abstract]. In: American Roentgen Ray Society 2018 Annual Meeting; 2018 Apr 22-27; Washington DC. Leesburg (VA): ARRS; 2018. Nr 1210.

9. Hyun Nam, W., Kang, D., Lee, D., et al. Automatic registration between 3D intra-operative ultrasound and pre-operative CT images of the liver based on robust edge matching. *Physics in medicine and biology*. 57. 69-91. 10.1088/0031-9155/57/1/69 (2011).

10. Volonté, F., Pugin, F., Buchs, N., et al. Console-Integrated Stereoscopic OsiriX 3D Volume-Rendered Images for da Vinci Colorectal Robotic Surgery. *Surgical innovation*. 20. 10.1177/1553350612446353 (2012).

11. Cui, N. & Kharel, P. & Gruev, V. Augmented reality with Microsoft HoloLens holograms for near infrared fluorescence based image guided surgery. In: Proc SPIE, vol 10049., pp 100490I-1–100490I-6, https://doi.org/10.1117/12.2251625 (2017).

12. Hanna, M. G., Ahmed, I., Nine, J., et al. Augmented Reality Technology Using Microsoft HoloLens in Anatomic Pathology. *Archives of Pathology & Laboratory Medicine*: May 2018, Vol. 142, No. 5, pp. 638-644. https://doi.org/10.5858/arpa.2017-0189-OA (2018).

Publishing Agreement

It is the policy of the University to encourage the distribution of all theses, dissertations, and manuscripts. Copies of all UCSF theses, dissertations, and manuscripts will be routed to the library via the Graduate Division. The library will make all theses, dissertations, and manuscripts accessible to the public and will preserve these to the best of their abilities, in perpetuity.

Please sign the following statement:

I hereby grant permission to the Graduate Division of the University of California, San Francisco to release copies of my thesis, dissertation, or manuscript to the Campus Library to provide access and preservation, in whole or in part, in perpetuity.

Author Signature

9/9/18

Date